Numerical simulations of embedded wrinkle defects geometry on the strength knockdown of FRP composites

Guglielmo Cimolai , Mehdi Yasaee [*]

School of Aerospace, Transport and Manufacturing, University of Cranfield, Cranfield MK43 0AL, UK

ABSTRACT

With the wide adoption of composite materials for a variety of applications, the prediction of their failure remains a challenging prospect. To complicate this scenario, out-of-plane fibre waviness defects, also known as wrinkle defects, are a major type of manufacturing defects that can degrade the mechanical performances of continuous carbon fibre composite panels, especially their compressive strength. In this work, the effects of such defects on square composite specimens are addressed through Finite Element (FE) analysis. A Matlab-Abaqus FE routine is proposed, which is capable of generating a wide variety of composite specimens with several types of embedded wrinkles and a number of controllable parameters. Parametric analyses are then performed to investigate the effects of defects characteristics on the knockdown in compressive strength, and several conclusions are drawn. Results show that is possible to determine the dependence of compressive strength on various wrinkle parameters such as amplitude or angle.

1. Introduction

With the wide adoption of composite materials in industry, used in a variety of different applications [1], the prediction of their failure remains a challenging prospect. This is in fact demonstrated by the various and not yet perfect failure criteria that have been proposed in the past, culminating in the World-Wide Failure Esercixes (WWFE) [2,3]. To complicate this scenario, internal defects such as variations of their mesostructure can occur in composite laminates as a result of manufacturing techniques [4], usually in the form of porosities, fibre misalignments, debonds or local variations in the fibre-volume fraction [5]. Failure of composite laminates under mechanical loading is strongly influenced by these types of defects [6]. One of the most commonly encountered defects is out-of-plane fibre waviness, commonly indicated as wrinkles [7], which appear on thick or curved laminates as bands of out-of-plane wavy plies. These types of defects can seriously degrade the mechanical performances of such laminates.

To describe the geometry of a standard out-of-plane wrinkle, various parameters can be adopted. The wave angle (commonly called wrinkle angle, θ), along with the amplitude A or the wavelength L, are common parameters used to describe typical fibre waviness [8]. Various studies have been conducted to experimentally characterize composite specimens with artificially induced wrinkle defects, manufactured by

inserting additional 90° prepreg strips to induce undulations in the laminate structure after curing [9]. Adams and Hyer [10], Wisnom and Atkinson [11] and Bradley et al. [12] made compression tests of wrinkled specimens using this process showcasing that shear stresses localized in the wavy region result in early matrix cracking and debonding. Lemanski et al. [13], Mukhopadhyay et al. [14] and Ferreira et al. [15] recognized the influence of wrinkle severity on the compressive failure strength. They found a 30% knockdown reduction of compressive strength for 12° angle waviness defects [14] and 54% for 22° ones [13] and built validated Finite Element (FE) models of such experimental tests for further analyses and confirmations [13,15].

From these studies, it has been highlighted the importance of understanding which wrinkle parameters, in terms of severity and extent, are most significant in the overall knockdown of mechanical performances of defected composites. This is important for practical applications, as to determine if and when components with such defects will still be safe to use or have to be eventually discarded. Various authors have investigated the characterisation of fibre waviness using non-destructive testing (NDT) by means of eddy current testing [16], X-ray computed tomography (CT) scan [17] or ultrasonic techniques [18] - the latter two more capable of 3D characterisation and therefore more suitable for industrial purposes, while the first one limited to more superficial defects. As demonstrated by Alghamdi et al. [19] and Makeev
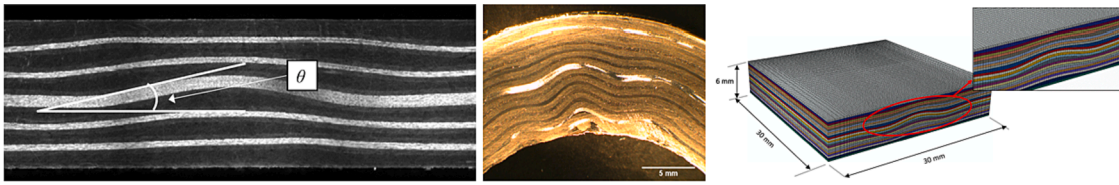
Fig. 1. (Left and centre) Examples of wrinkle defects in composite laminates; (right) FE model of the waviness defect in a composite specimen. Source: images extracted from [14].

and Nikishkov [20], measured properties of X-ray CT data can be used to produce accurate FE models of wrinkled specimens which can provide a good predicting capability for performance. Freemantle et al. [21], Sandhu et al. [22] and Smith et al. [23] created damage maps starting from ultrasonic B-scan data and used them to validate proposed FE models.

Composite laminates with embedded wrinkle defects subjected to compressive stress states show complex failure mechanisms involving both intra-laminar and inter-laminar damages, i.e. fibre breakage, matrix cracking and delaminations [14]. Many models have been proposed in the past to numerically describe these kinds of damages in FE analysis frameworks. In the present work, intra-laminar damages are considered by means of the failure criteria proposed by Hashin and Rotem in [24], which is capable of treating fibre breakage in tension, fibre buckling in compression, and matrix cracking and crushing due to shear and tension/compression. For the onset of inter-laminar damages (delaminations), the Cohesive Zone Method (CZM) approach has been chosen, which is based on the theoretical work about cohesion of Dugdale [25] and Barenblatt [26]. It is mathematically described by a Traction-Separation Law coupled with a quadratic damage initiation criterion [27], and a power-law criterion is used to govern the mixed-mode behaviour damage evolution [28].

As said, the significance of wrinkle defects in composite structures has been demonstrated by both experimental and numerical analyses available in the literature, and the importance of their evaluation in quality control of manufacturing has been highlighted. Nonetheless, there is still uncertainty on which parameters have the most considerable influence on the detrimental effects of such defects, in particular on compressive strength. As highlighted before, different authors have proposed the amplitude A, the wavelength L or the wrinkle angle θ as candidates for mathematically describing wrinkle severity. In particular, Lemanski et al. [13] and Mukhopadhyay et al. [14] have proposed the maximum angle as a defining parameter, while as another example, Fedulov et al. [29] used the height of the wave. Moreover, Hsiao and Daniel [30] used the wavelength, Caiazzo et al. [31] used the amplitude

and El-Hajjar and Petersen [32] proposed a gaussian bell to model the wave, also defined in terms of amplitude.

From the literature analyzed a missing consensus emerges on the effect of defect geometry on structural performance. Therefore, there is a need for a parametric study of wrinkle defects, to understand the influence of different parameters and their consequent importance. This can give industrial guidance for the NDT of manufactured composite components in the quality-control phases. Such comprehension has been not achieved completely in the past due to the difficulties associated with both manufacturing induced wrinkle defects with controllable parameters for testing and validation purposes and creating large numbers of FE models of such defects to perform extensive numerical analyses. In the present paper, a newly developed Matlab routine is presented which has the capability to produce FE models of a wide variety of wrinkled specimens to be imported and analysed in Abaqus/Explicit. Using this tool, a parametric study is performed to explore the wrinkle parameter space and understand the influence of different parameters on the compressive failure strength of wrinkled composite laminates. A detailed discussion of wrinkle geometry effects on tensile and compressive loading, wrinkle angle and amplitude as well as embedded wrinkles with flat or non-flat laminates are presented. Finally, experimental validation is performed by comparing the obtained numerical results with experimental data on identical models available in the literature. The numerical model proposed aims to simulate the behaviour of square composite specimens with embedded wrinkles generated from a variety of defects with controllable characteristic using a versatile automative tool to generate models with different types of defects. The primary purpose of this tool is to provide a parametric analysis of different defect characteristics to understand their relative importance on the strength knockdown in both tension and compression loading. The viability of the proposed procedure for application in industrial testing will be evident, showcasing capability to numerically assess the acceptability criteria of defected composite parts which can help reduce costly scrapping/repairing of manufactured parts.
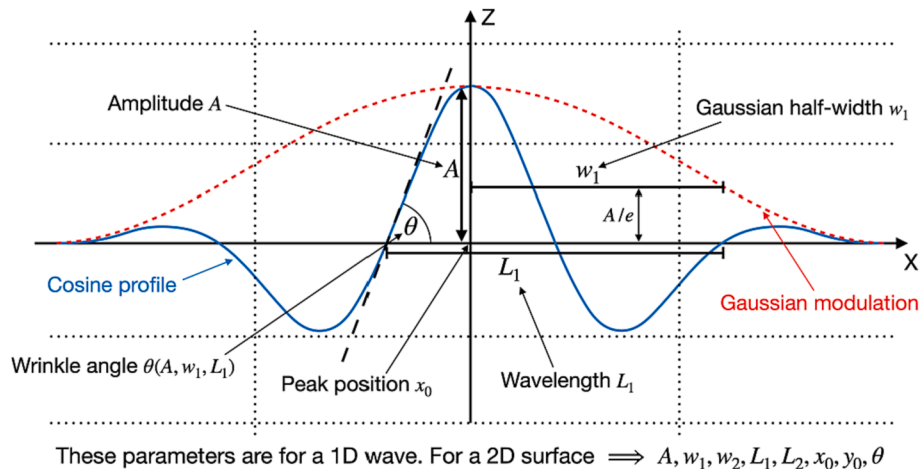
Fig. 2. Definition of wrinkle parameters for the proposed mathematical model of the waviness defect. The definition of such surface is expressed in Eq. (1), which outlines a relationship between the following eight wrinkle parameters (highlighted in Fig. 2, for the x-z projection only):
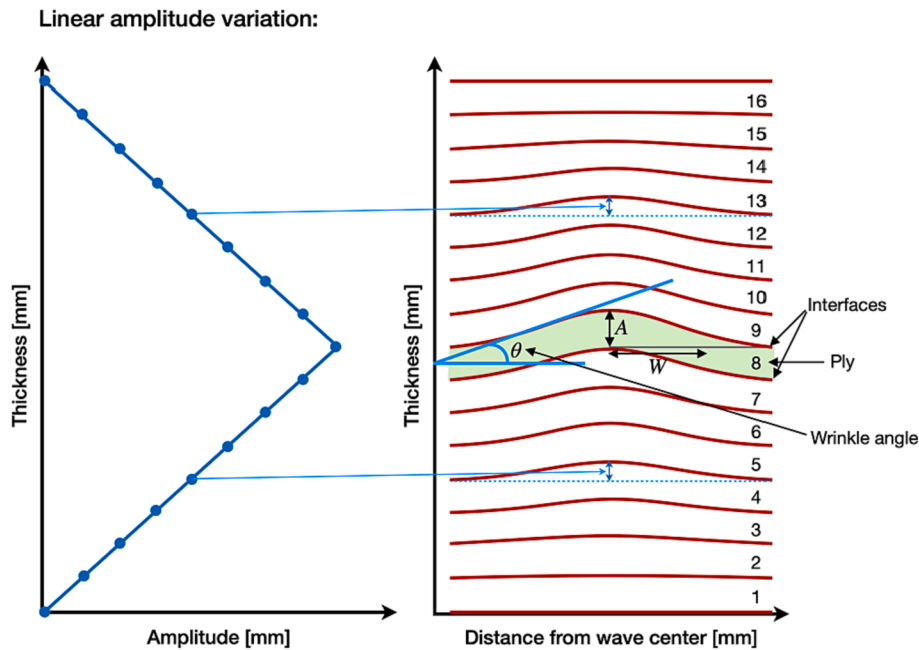
Linear amplitude variation:

Fig. 3. Linear through-the-thickness amplitude variation, with visualization of the wrinkle angle definition.

The paper is organized as follows: Section 2 the numerical tool is presented, with the definition of wrinkle parameters and their pro- grammatic implementation as well as the characterization of the pro- posed FE models. Section 3 then presents the results from the parametric study performed, where several wrinkle parameters are addressed. Finally, in Section 4 the obtained results are discussed, and several conclusions are drawn, together with the experimental validation of the numerical model.

2. Scripted wrinkle generation numerical model

For the generation, and successive Abaqus implementation, of high- fidelity models of wrinkled specimens a Matlab routine has been developed, capable of generating a detailed ply-by-ply model of a wrinkle-defected composite specimen in a form of a.*inp* input file. The wrinkle's geometry is defined using a simple yet realistic mathematical description of the wrinkle waviness, implemented through a small set of parameters capable of generating a wide class of defect geometries with controllable characteristics. A collection of images representing wrinkle defects in composite laminates and their corresponding FE models is shown in Fig. 1.

2.1. Mathematical model representation of the wrinkle shape

The mathematical model of the defect's topology, which describes the typical undulation shape using a three-dimensional cosine surface modulated by a Gaussian envelope, has been chosen based on the analysis outlined in [4]. This model will define the curved surface of a generic ply inside the laminate. The intersection of such type of surface with the x-z plane is shown in Fig. 2 (y-z projection follows the same trend), where its defining parameters are highlighted. From this point the x-axis will be taken as the reference direction for 0° plies, and will also be referred to as load-axis.

- θ- Wrinkle angle;
- A- Maximum ply amplitude;
- L_1 and L_2 - Wavelengths in the x and y-directions respectively;
- w_1 and w_2 - Wrinkle gaussian half-widths in the x and y-directions respectively;
- x_0 and y_0 - Wrinkle centre location coordinates.

$$f(x,y)_{top} = A_1 \cdot e^{\left(-\frac{(x-x_0)^2}{w_1^2}\right)} cos(2\pi \frac{x-x_0}{L_1}) \cdot e^{\left(-\frac{(y-y_0)^2}{w_2^2}\right)} cos(2\pi \frac{y-y_0}{L_2})$$

$$f(x,y)_{bottom} = t + A_2 \cdot e^{\left(-\frac{(x-x_0)^2}{w_1^2}\right)} cos(2\pi \frac{x-x_0}{L_1}) \cdot e^{\left(-\frac{(y-y_0)^2}{w_2^2}\right)} cos(2\pi \frac{y-y_0}{L_2})$$

(1)

It is noticeable how for creating a single ply two different surfaces need to be defined in Eq. (1), representing the upper (top) and lower (bottom) surface. These surfaces are characterized by two different maximum amplitude values, A_1 and A_2, in order to take into account the through-the-thickness variation of the wrinkle severity inside the lami- nate. The two surfaces are separated (in the z-direction) by the pristine ply thickness t, which can be individually defined for each ply. The ply bulk material is therefore defined based on the volume between the two surfaces, with homogenized material properties assigned to it.

2.2. Through-the-Thickness variation of wrinkle severity

For modelling the through-the-thickness amplitude variation, the implemented routine creates a suitable set of interpolation values taking into account both the desired min and max values of amplitude. These are the amplitude values at the two external surfaces and at the centre, respectively. It then considers the number of plies in the laminate and the ply thickness values for the various plies and assigns the interpolated amplitude values at the successive interply surfaces. This is to obtain the maximum selected value of amplitude in the centre of the laminate, guaranteeing at the same time perfect contact between the various plies. Different types of interpolation can be potentially defined (linear, Gaussian, stepped, etc).

2.3. Wrinkle angle definition

The wrinkle angle θ is not directly appearing in Eq. (1). The reason is that the wrinkle angle is not an independent parameter that can directly define the wrinkle shape, but it is a function of amplitude, wavelength and gaussian half-width in the longitudinal direction: $\theta = \theta(A, L_1, w_1)$ [4]. Simplifying the angle definition by considering the parameter $L_1 \to \infty$, so that the gaussian half-width w_1 can replace the definition of the wavelength parameter, a fixing of one of the two parameters (amplitude A and wavelength w_1) is required to solve the nonlinear
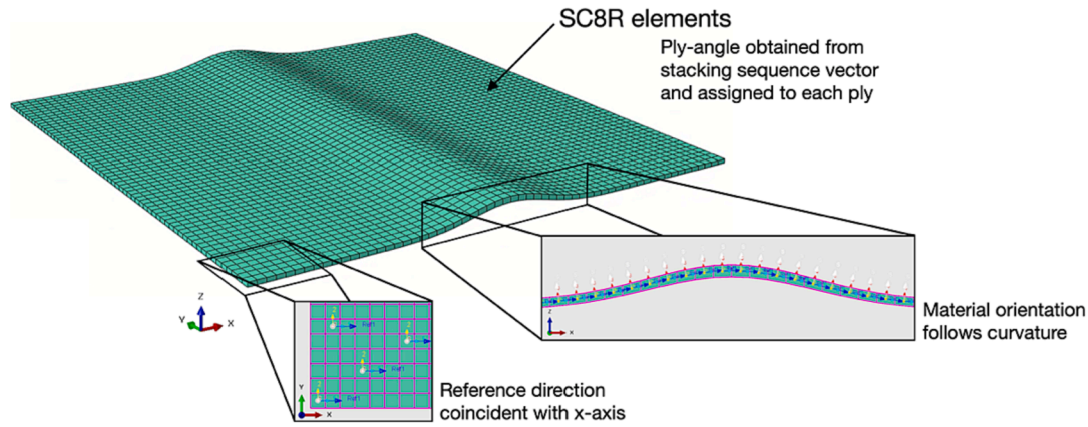
Fig. 4. Mesh and material orientation definition for the generic curved ply.

equation $\theta = \theta(A, w_1)$. Requesting the user to define both the desired angle θ and one of the two parameters, between amplitude A and wavelength w_1, the second missing parameter can be calculated by an iterative process and the obtained couple (A, w_1), satisfying the requested angle θ, can be therefore used in creating the various plies. The definition of the wrinkle angle θ is based on taking the arctangent of the first directional derivative of the wave function in the point of curvature change, i.e. zero of the second derivative, mathematically:

$$\theta = tan^{-1}(max(\frac{\partial f(x, y)}{\partial x})) \tag{2}$$

where the function f in Eq. (2) is obtained from the upper surface definition in Eq. (1).

Summing the results of the two previous paragraphs, an example of the linear amplitude variation, with the visualization of the wrinkle angle definition, is shown in Fig. 3.

2.4. Global script generation

A conceptual representation of the workflow followed by the Matlab routine is contained in Appendix 1, divided into two parts: 1) Laminate configuration, 2) Wrinkle generation. In the laminate configuration phase, the user is asked to define the stacking sequence and the ply thickness(es) value(s). In the wrinkle generation phase, the user can select different defining parameters (angle, amplitudes, etc), and different subroutines will generate the desired defect. As represented in Appendix 1, different alternative paths can be followed for generating the defect, giving therefore multiple possibilities to the user. Several types of embedded wrinkle defects will be studied in the next Section 3 and will be briefly presented in Section 2.6.

2.5. FE model description

2.5.1. Material and section properties

For implementing section properties of each ply a one-ply continuum shell section is defined using the Abaqus *composite layup tool,* with the definition of a relative thickness of 1. The ply is meshed with quadrilateral 8-noded continuum shell elements (SC8R elements in Abaqus), with reduced integration, hourglass control and finite membrane strains. The correct ply-angle is extracted from the defined stacking sequence vector and assigned to each ply (reference direction for the ply orientation coincident with the x-axis), with three through-the-thickness integration points and the correct material orientation and stacking direction - essential for performing simulations involving curved fibres - as represented in Fig. 4. Relative to the simulations performed in the following Section 3 each ply has been meshed with one element through-the-thickness, and an element size of 0.5x0.5 mm has been set

Table 1

Unidirectional carbon-epoxy Hexcel® IM7/8552 material properties. Source: data extracted from [34,35].

Mechanical Properties		Strength Properties		Damage Evolution Properties	
ρ	1570 kg/m^3	X^T	2300 MPa	Type	Energy
E_{11}	161.0 GPa	X^C	1000 MPa	Softening	Linear
$E_{22} = E_{33}$	11.38 GPa	Y^T	62.3 MPa	G_I^T	10 kJ/m^2
$G_{12} = G_{13}$	5.17 GPa	Y^C	253.7 MPa	G_I^C	10 kJ/m^2
G_{23}	3.92 GPa	S^L	89.6 MPa	G_{II}^T	290 J/m^2
$\nu_{12} = \nu_{13}$	0.32	S^T	126.9 MPa	G_{II}^C	290 J/m^2
ν_{23}	0.3813	α	0	η	10^(-6)

by default together with a ply thickness of 0.125 mm. The side dimensions for the square specimen are chosen as 30x30 mm. A homogeneous unidirectional carbon-epoxy Hexcel® IM7/8552 resin/fibre material, possessing a fibre volume fraction of $V_f = 57.70\%$ [33], has been implemented with the mechanical properties extracted from [34,35] and outlined in Table 1. Assembly of the wrinkled laminate is then performed by superimposing the individually created plies, meaning that the various plies – each modelled as an individual part in Abaqus, with its own geometry, mesh and section properties – are stacked on top of each other to form the laminate, with contact properties defined to model the cohesive behaviour. This modeling technique allows capability to capture delamination between plies, a critical failure mechanism that initiates from fibre waviness defects. A representation of the assembly strategy is shown in Appendix 2.

2.5.2. Intralaminar damages

Damage occurrence for the individual plies of the composite laminate (intralaminar damages) has been considered by means of the Hashin Failure Criteria [24], which is suitable for treating damages in anisotropic materials since it considers four different failure modes for both fibre and matrix in tension and compression, i.e. fibre breakage in tension, fibre buckling in compression and matrix cracking and crushing due to shear and tension/compression. It relies on damage initiation parameters indicated as X^T, X^C, which represent longitudinal tensile and compressive strengths, Y^T, Y^C, which represent transverse tensile and compressive strengths, S^L, S^T, which represent longitudinal and transverse shear strengths, and an additional parameter α representing the influence of shear stress on the fibre tension criterion.

After damage onset has occurred for at least one of the four conditions, damage evolution is treated with the use of an energy-type degradation behaviour with linear softening, suitable for describing stiffness degradation of the material after at least one of the four Hashin's criteria is met [36], through the definition of tensile and
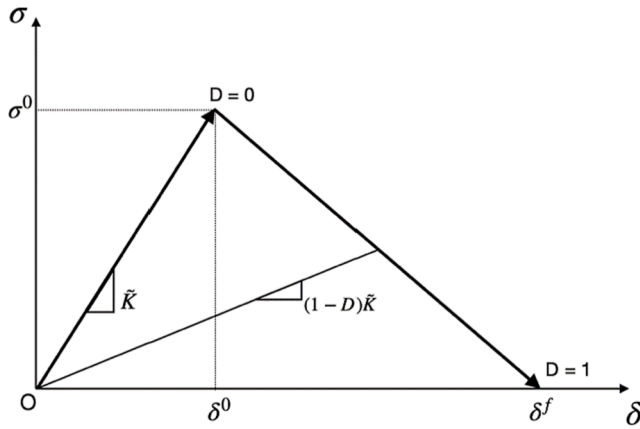
Fig. 5. Bilinear Traction-Separation Law for the definition of cohesive contact between plies.

compressive fracture energies G_I^T, G_I^C in longitudinal direction and G_{II}^T, G_{II}^C in transverse direction. These energies represent the fracture energies needed for the damage propagation after its onset and are therefore directly related to the four initiation criteria, while the linear softening represents a linear degradation of the stiffness of the damaged material. Damage stabilization has been also considered by the definition of a viscosity coefficient η. The outlined strength and damage evolution properties, extracted from [34,35], are collected in Table 1, together with the mechanical ones previously cited.

2.5.3. Interlaminar damages

A general contact interaction has been defined with a hard-contact behaviour applied on all external surfaces, while a cohesive behaviour has been defined between each interply surface by making use of the Cohesive Zone Method (CZM) approach for considering inter-laminar damage occurrence. Based on the theoretical work about cohesion theory of Dugdale [25] and Barenblatt [26], the Cohesive Zone Method (CZM) relies on the definition of a Traction-Separation Law (*T*-S Law), usually expressed in a bilinear form such as that shown in Fig. 5, which is a relation between the stress components σ acting at the interface between two neighbouring plies, and the separation components δ defined between the two interfaces due to delamination onset and evolution [27,28].

The purpose of the *T*-S Law is to account for the progressive loss of stiffness in the damaged interface, since damage can be considered as a progressive phenomenon, for which the ability of the cohesive interface to sustain loads is not completely lost at damage onset [37]. For implementing the bilinear curve, a linear elastic behaviour is first defined through the use of a penalty stiffness coefficient $\widetilde{K}$, until the interfacial strenght indicated by σ^0 is reached, which represents the point of damage onset [27]:

$$\sigma = K\delta \rightarrow K = \left\{ \begin{array}{l} \widetilde{K}, \delta \leq \delta^0 \\ (1-D)\widetilde{K}, \delta^0 < \delta \leq \delta^f, D \in [0,1] \end{array} \right. \tag{3}$$

Where D is the damage variable that ranging from 0 to 1 – 0 indicating pristine material and 1 the completely damaged interface –, accounts for the progressive evolution of delamination damage, and δ^0 can be expressed as $\delta^0 = \sigma^0/\widetilde{K}$.

After damage onset, a progressive degradation is followed, with the

stiffness of the cohesive interface being progressively lowered until the maximum displacement δ^f is reached and delamination advances:

$$D = \left\{ \begin{array}{l} 0, \delta \leq \delta^0 \\ 1, \delta = \delta^f \end{array} \right. \tag{4}$$

For the calculation of the maximum displacement δ^f, an energetic consideration is needed: since from the cohesion theory it is known that delamination grows when a suitable fracture toughness value is reached [38], the area under the bilinear law must be equal to that value of strain energy, and therefore δ^f can be expressed, taking into account the value related to the particular delamination mode considered (I, II, III or mixed) as:

$$\delta^f = 2G/\sigma^0 \tag{5}$$

The cohesive contact behaviour has been implemented in Abaqus defining damage initiation by means of the quadratic stress criterion (QUADS criterion in Abaqus) [38], with interfacial strength values σ_I^0, $\sigma_{II}^0 = \sigma_{III}^0$ and fracture energies $G_{IC}, G_{IIC} = G_{IIIC}$ (for simplicity Mode III strength and toughness are considered the same as Mode II). The QUADS criterion, which works well for mixed-mode conditions since it interrelates all three critical tractions defined, is met when the following relationship holds [38]:

$$\left(\frac{\sigma_I}{\sigma_I^0} \right)^2 + \left(\frac{\sigma_{II}}{\sigma_{II}^0} \right)^2 + \left(\frac{\sigma_{III}}{\sigma_{III}^0} \right)^2 = 1 \tag{6}$$

The damage evolution has been treated by specifying an energy type evolution with a power-law description based on the Benzeggagh-Kenane mixed-mode behaviour [39] which makes use of a coefficient $BK = 2.1$ and permits the treatment of mixed-mode delaminations involving mode I, II and III types. The cohesive properties utilized are extracted from [34] and reported in Table 2.

2.5.4. Boundary conditions

To perform tensile and compressive simulations of wrinkled laminates which are characterized by convoluted geometries, and due to the complex contact interactions and failure behaviours involved in the FE modeling, a dynamic explicit step has been defined, with a target time period of 0.1 s. Nonlinear geometry has been activated to take into account the severe deformations involved, and mass-scaling has been defined with a target time increment of 10^{-6} s to help speed up the computational time. This time has been carefully selected to ensure that kinetic energies remain below 5% of total energies so as not to influence the fracture behaviour with spurious stress oscillations and dynamic effects, effectively producing a quasi-static loading response.

For the application of imposed displacements to the laminate a smooth-step amplitude has been created, and one of the two faces in the y-z plane of the laminate has been completely fixed by constraining all nodes' six degrees of freedom in the surface. On the opposite face, all nodes have been given an imposed displacement in the loading direction with the sign determining if the load is in tension or in compression, while the other degrees of freedom have been fixed, as shown in Fig. 6. For computing compressive strength values, the reaction force outputs have been requested on all the nodes of the loaded side and, for visualization purposes, the cohesive contact damage field variable (CSDMG variable in Abaqus) has been activated to visualize the delamination contour plots.

Table 2
Cohesive interfacial properties. Source: data extracted from [34].

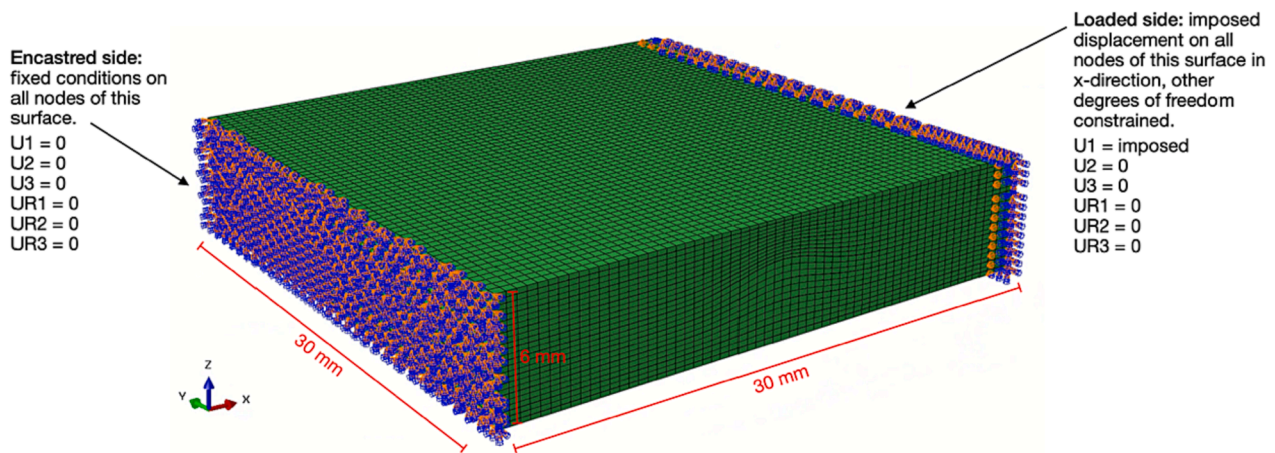| σ_I^0	σ_{II}^0	σ_{III}^0	G_I	G_{II}	G_{III}	Type	Mixed-mode behavior	BK
15 MPa	340 MPa	340 MPa	210 J/m^2	663 J/m^2	663 J/m^2	Energy	Bezeggagh-Kenane	2.1

Fig. 6. Boundary conditions applied to a generic laminate for performing tensile and compressive simulations.

2.6. Wrinkle model generation demonstration

A brief description of several possible wrinkle geometries that can be defined by the present tool is contained in this paragraph, to highlight key features and capabilities that will be further developed in the next section. Fig. 7 presents a collection of defected square specimens together with the defined wrinkle parameters as per Section 2.1. The simplest type of defect, Fig. 7(a, b, c) is constituted by a bi-dimensional single wave extruded with a constant profile, which will be reffered to as a *Full-wave* defect and that can be used to address the effects of angle and amplitude severity on the knockdown effect. The amplitude variation between successive couple of plies can be governed by a linear or Gaussian evolution or, more realistically, a stepped one which is particularly useful for describing wrinkle defects resulting from the autoclave process [14]. By reducing the amplitude of the Full-wave defect in the extrusion direction, a *Bulge* defect is obtained, Fig. 7(d), which is not visible from the outside since the wave has been constrained to remain inside the laminate, having a maximum amplitude at the centre. The previous defects have been shown to have flat top and bottom surfaces: this is not always the case, as in real scenarios the vacuum bagging used for curing composites in the autoclave will make wrinkle defects appear on the upper surface [40]. Non-flat type of defects can therefore be defined as in Fig. 7(e). Finally, complex stacking sequence definitions can be managed by the tool, particularly in the case of non-uniform ply-thicknesses as in Fig. 7(f).

3. Parametric study of wrinkle defect

In this section, FE simulations conducted on various square wrinkled specimens generated by the implemented Matlab routine are described. Results are shown and compared to gain an understanding of the influence of different wrinkle defects on the tensile and compressive failure behaviour of such laminates. A quasi-isotropic 48-plies laminate of carbon-epoxy IM7/8552 material has been considered, with a stacking sequence of $[45_2/90_2/-45_2/0_2]_{3S}$ and nominal ply thickness of 0.125 mm. To save computational time, successive couple of plies with the same ply-angle have been merged as a single ply and therefore a 24-plies laminate with $[45/90/-45/0]_{3S}$ stacking sequence and ply thickness of 0.250 mm has been modelled. Such quasi-isotropic layup has been chosen as representative of layups used in industrial practice [14]. The considered specimens are 30x30 mm squares with a total laminate thickness of 6 mm, meshed with 0.5x0.5 mm element size, for a total of 86,400 SC8R elements simulated.

For identification purposes, simulations have IDs in the form "*N*-F/B-M", where N is the wrinkle angle in degrees, F/B indicates the type of defect that could be *Full-wave* or *Bulge*, and M is the maximum amplitude in terms of ply thicknesses (eg. 10F5 means 10° wrinkle angle, Full-wave

type defect, maximum amplitude equals to 5 plies, or 5x0.125 mm = 0.625 mm). An outline of the performed analyses is contained in Fig. 8. For representing the simulation results, various plots of the stress-displacement response are collected in this section. For qualitative comparison between the different models analyzed, the delamination damage contour plots at different stages of the loading have been presented by means of the CSDMG variable in Abaqus. The different stages were selected based on general trends or to capture specific behavior observed, such as initiation of delamination damage and damage pattern before and after significant load drops. These points have been associated to specific points in the stress-displacement plot for each specimen for ease of identification using IDs in Fig. 8.

3.1. Tensile and compressive loading

In the first set of simulations, comprising the four simulations *BenchT*, *BenchC*, *15F5T* and *15F5C*, tensile (T) and compressive (C) analyses have been performed on both a pristine model (Benchmark) produced by inputting a 0° angle in the wrinkle generation phase, and a 15° wrinkled specimen with a defined amplitude of 0 mm on external edges (flat top and bottom surfaces) and 0.625 mm on the central layer, equal to 5 times the ply thickness' original value. The defected laminate has a single full-wave type of defect, consisting of a constant wrinkle profile along the specimen's width (therefore visible from the outside frontal and rear faces). These simulations are performed in order to quantify the strength reduction effect for a medium/high-severity defect. Results from such simulations are collected in Fig. 9.

In the tensile tests of Fig. 9 the benchmark model initially failed at the specimen ends, where the boundary conditions have been applied; the damage then propagated towards the centre of the specimen as the applied displacement increased. The wrinkled laminate shown an initially localized delamination at the centre of the laminate where the wave has been positioned, which then propagated towards the loading ends. In both cases, failure occurred in the + 45/-45° interfaces and in the 90° ones, triggered by matrix cracking and shear stresses as expected. Regarding the compressive tests of Fig. 9, the benchmark model shown a clear crushing failure happening towards the encastred side. The wrinkled laminate again shown an initially localized failure correspondent to the defect's centre subsequently evolving towards the two sides, thus encompassing the whole laminate and producing visible multiple delaminations and bulging of the upper surface.

3.2. Wrinkle angle variation

In the second set, comprising the six simulations *5F5*, *10F5*, *12F5*, *15F5*, *15B5*, *20F5*, compressive tests have been performed on 5°, 10°, 12°, 15° and 20° wrinkled laminates, with a single full-wave type of
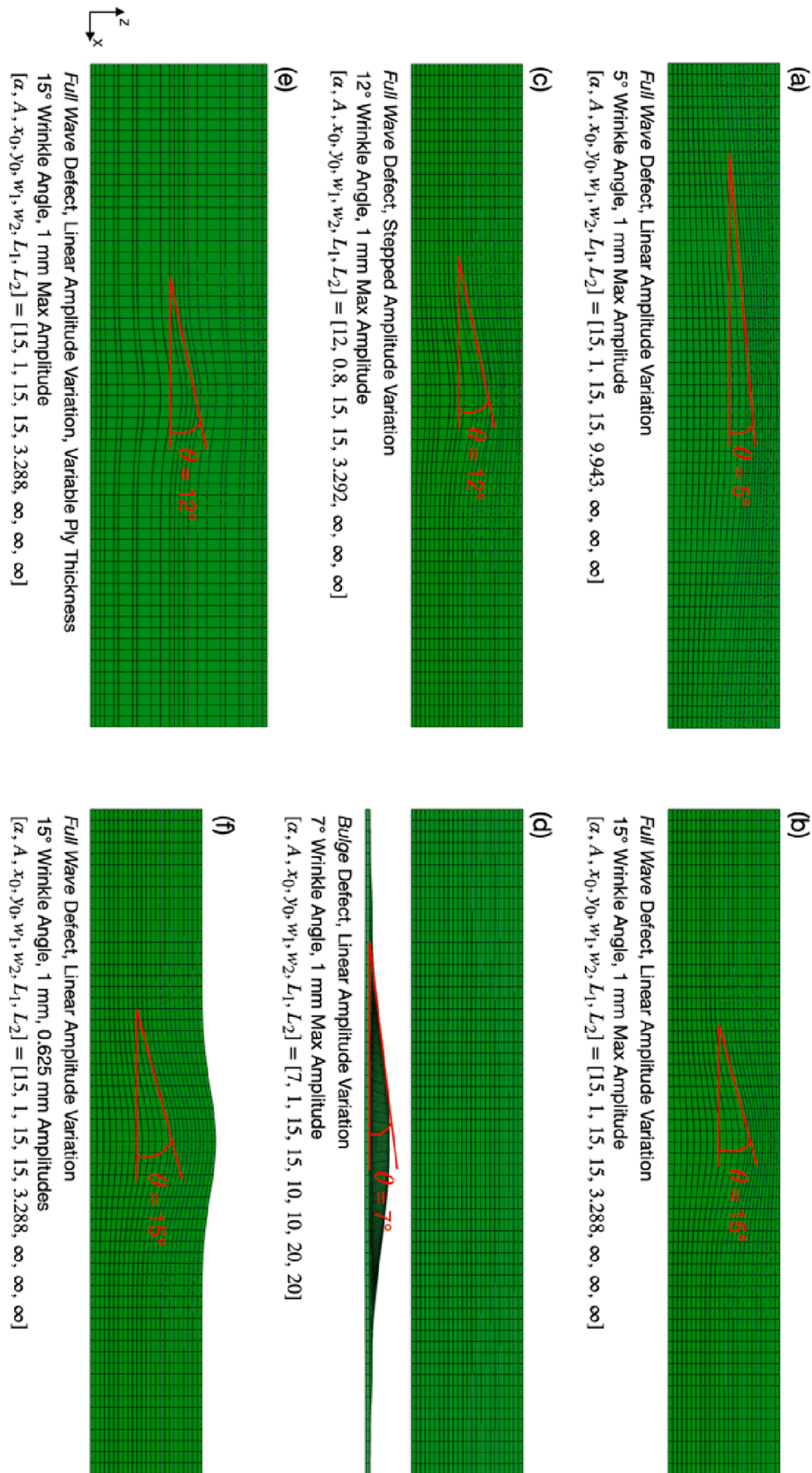
Fig. 7. Capabilities of the implemented Matlab routine in terms of defect variations. (a, b) *Full-wave* defects with linear amplitude variation and different severities (a – low angle, b – high angle); (c) *Full-wave* defect with stepped amplitude variation; (d) *Bulge* defect with linear amplitude variation and central ply represented; (e) *Full-wave* defect with unequal thickness laminate; (f) *Full-wave* defect with non-flat upper surface.

Laminate Configuration			Wrinkle Defect Configuration				Simulation Data			Set
Stacking Sequence (Number of Plies)	Ply Thickness	Laminate Dimensions	Wrinkle Angle	Amplitudes**	Type of Defect	Wrinkle Parameters $[x_0, y_0, w_1, w_2, L_1, L_2, s, r]$	ID Name	Load Type	CPUs used / CPU time ‡	
$[+45_2/90_2/-45_2/0_2]_{3S}$ (48 plies)*	0.125 mm*	30×30×6 mm	0°	Not Defined***			BenchT	Uniaxial Tension	16 / 03:06:55 h	Set 1
			0°	Not Defined***			BenchC	Uniaxial Compression	16 / 03:02:56 h	Set 1
			15°	0 mm, 0.625 mm	Full Wave†	[15, 15, 2.0550, ∞, ∞, ∞, 30, 0.5]	15F5T	Uniaxial Tension	16 / 02:36:28 h	Set 1
			15°	0 mm, 0.625 mm	Full Wave†	[15, 15, 2.0550, ∞, ∞, ∞, 30, 0.5]	15F5C	Uniaxial Compression	16 / 02:40:04 h	Set 1
			5°	0 mm, 0.625 mm	Full Wave	[15, 15, 6.2140, ∞, ∞, ∞, 30, 0.5]	5F5†††	Uniaxial Compression	16 / 02:16:33 h	Set 2
			10°	0 mm, 0.625 mm	Full Wave	[15, 15, 3.0890, ∞, ∞, ∞, 30, 0.5]	10F5		16 / 02:35:18 h	Set 2
			12°	0 mm, 0.625 mm	Full Wave	[15, 15, 2.5710, ∞, ∞, ∞, 30, 0.5]	12F5		16 / 02:43:41 h	Set 2
			15°	0 mm, 0.625 mm	Full Wave	[15, 15, 2.0550, ∞, ∞, ∞, 30, 0.5]	15F5		16 / 02:40:04 h	Set 2
			15°	0 mm, 0.625 mm	Bulge††	[15, 15, 2.0550, 7.5, ∞, ∞, 30, 0.5]	15B5		16 / 02:52:46 h	Set 2
			20°	0 mm, 0.625 mm	Full Wave	[15, 15, 1.5400, ∞, ∞, ∞, 30, 0.5]	20F5		16 / 02:43:06 h	Set 2
			15°	0 mm, 1 mm	Full wave	[15, 15, 3.2880, ∞, ∞, ∞, 30, 0.5]	15F8		16 / 02:31:57 h	Set 3
			15°	0 mm, 0.625 mm	Full wave	[15, 15, 2.0550, ∞, ∞, ∞, 30, 0.5]	15F5		16 / 02:40:04 h	Set 3
			15°	0 mm, 0.250 mm	Full wave	[15, 15, 0.8220, ∞, ∞, ∞, 30, 0.5]	15F2		16 / 02:55:03 h	Set 3
			15°	0 mm, 1 mm, 0.500 mm	Full wave	[15, 15, 3.2880, ∞, ∞, ∞, 30, 0.5]	15F84nf		16 /	Set 4
			15°	Amplitude vector[a]	Full wave	[15, 15, 3.2880, ∞, ∞, ∞, 30, 0.5]	Stepped		16 /	Set 4

* Approximated to a 24-plies laminate by merging successive couple of plies, obtaining therefore an effective ply thickness of 0.250 mm.

** If two numbers are shown, the first refers to the external upper and lower laminate's surface amplitudes and the second to the central surface (laminate midplane) and the third to the upper external surface. A linear amplitude variation is assumed unless specified.

*** For the benchmark model which represents the pristine laminate, the wrinkle defect is not defined, therefore the amplitudes are 0mm on both the external surfaces and the midplane and the wrinkle parameters are indeterminate. (s, r) are equal to (30, 0.5) nonetheless.

† The Full Wave defect represents a constant wrinkle profile with a single wave, extruded along the width of the specimen, perpendicular to the loading direction.

†† The Bulge defect represents a constrained wave inside the laminate, thus guaranteeing pristine external edges and faces.

††† The defects are categorized with a construct in the form N-F/B-M, where N is the wrinkle angle in degrees, F/B indicate if the defect is a Full-wave one or a Bulge one, and M indicates the amplitude in terms of the original ply thickness value. 5F5 represents therefore a 5° wrinkle angle, Full-wave, 0.625mm max amplitude defect (pedices can be added, like T for Tension, C for Compression, nf for non-flat external surface).

[a] Stepped amplitude variation with the following values between successive interplies, starting from the bottom of the laminate: [0, 0.1, 0.3, 0.3, 0.3, 0.5, 0.5, 0.7, 0.8, 0.8, 0.7, 0.5, 0.5, 0.5, 0.5, 0.3, 0.3, 0.3, 0.3, 0.1, 0].

‡ Cranfield University's Crescent HPC used for performing simulations. Cpus utilized are Intel® Xeon® E5-2660, simulation time has been extracted from the .sta ABAQUS™ file at last time increment and comprises both the total simulation time and the parallelization time. Queue time is not considered, therefore the actual time spent on simulation is generally higher. 16 cpus have been chosen to maintain parallelization time low and perform multiple simulation at the same time.

Fig. 8. Overview of the performed simulation studies.
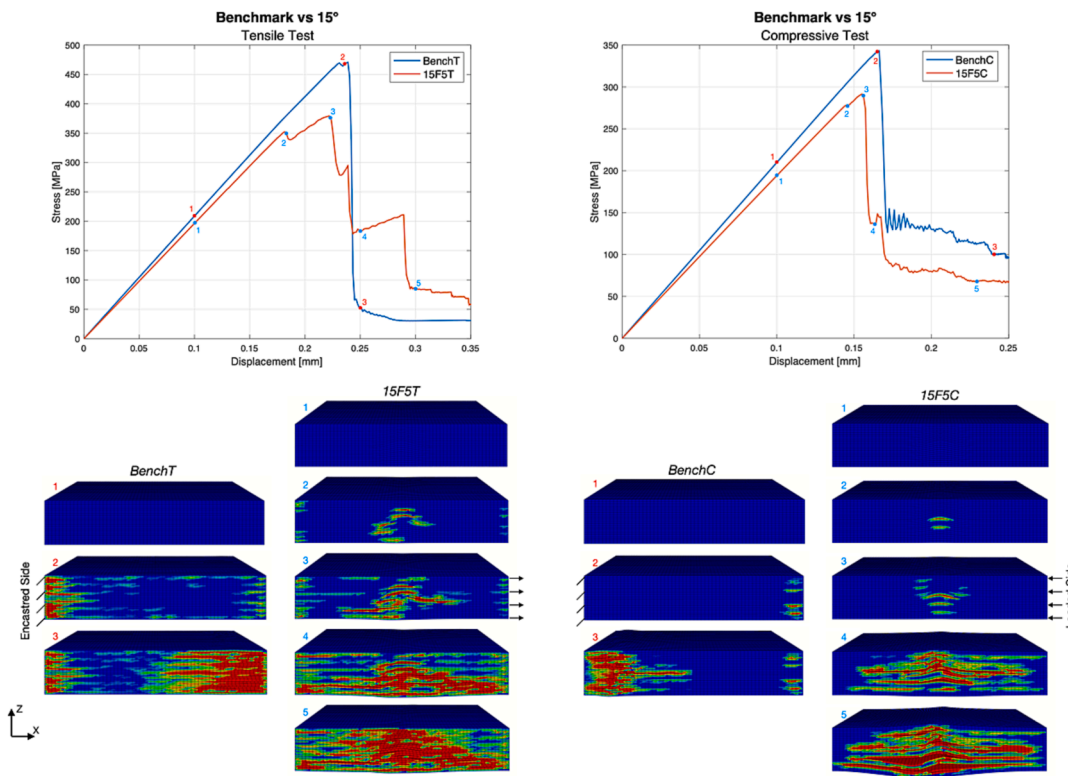
Fig. 9. Pristine benchmark model vs 15° wrinkle model with 0.625 mm amplitude. (Left) tensile simulation; (right) compressive simulation. Delamination contour plots at critical moments are represented by means of CSDMG damage field variable, with blue color indicating pristine material and red color complete delamination. (For interpretation of the references to color in this figure legend, the reader is referred to the web version of this article.)

defect (F simulations) or internal bulge defect (B simulation). Flat top and bottom surfaces have been considered for all simulations. These simulations are conducted to understand the effects of the wrinkle angle on the compressive strength reduction, for a constant max amplitude. As part of the second set of simulations, a comparison between the full-wave type of defect and the bulge defect has been performed relative to the 15° angle case, this time by constraining the defect to remain inside the specimen for producing a bulge-type defect to be compared with the full-wave type. Results from such simulations are collected in Fig. 10 and Fig. 11. The analysis of the compressive tests performed on the wrinkled laminate by modifying the wrinkle angle shows that the failure behaviour maintains the same characteristics between the various angles. Initial localized failure is triggered by Mode II delaminations occurring between the −45° and 0° ply, which then extends suddenly to the whole laminate due to instability failure between plies, at the compressive strength level. As noticeable from the analysis of the different behaviour between full-wave and bulge defects, the diminished cross-sectional area of the bulge defect in the loading direction has a clear effect on the compressive strength.

3.3. Wrinkle amplitude variation

In the third set, comprising the three simulations *15F2, 15F5, 15F8*, compressive tests have been performed on 15° wrinkled specimens with a full-wave type of defect by varying the maximum amplitude, equal in these cases to 0.250 mm, 0.625 mm and 1 mm, to understand the effect of varying amplitude for constant wrinkle angle. Results from such simulations are collected in Fig. 12. As noticeable from the analysis of Fig. 12, the influence of the wave amplitude on the compressive strength is not negligible.

3.4. Flat vs Non-Flat surface and stepped amplitude variation

The defects shown in the previous section were idealized for the purpose of addressing the effects that the governing parameters singularly had on the knockdown of defected specimens. For validating the proposed numerical model and the presented results, a comparison with experimental data available in the literature will be performed in the next paragraph (see Section 4.1 – Validation of the Numerical Models), which will require more realistic defects to be considered. In fact, defects embedded on real specimens such as those produced by inserting pre-preg strips inside the manufactured components in the 90° laminate direction, show a specific shape that can be approximated by a stepped model [4,14]. Frequently, due to the rigid tooling and the vacuum bagging used for curing composites in autoclave, wrinkle defects appear on the upper surface (while the lower one is in contact with the rigid tool and thus ends up being flat) [40]. To address this phenomenon, the last set of two simulations have been proposed with a 15° wrinkle angle investigated for comparison purposes with previous results. The first is a non-flat upper surface defect with linear amplitude variation between plies, the second a stepped model where successive groups of [-45°, 0°, 45°] plies possess the same amplitude value, and the 90° plies present subsequent amplitude variation to permit the overall through-the-thickness amplitude evolution. Results from such simulations are collected in Fig. 13.

4. Discussion of results

From the analysis of the previous results, different conclusions can be drawn. In the tensile tests of Fig. 9, the stress-displacement plots show a clear difference in behaviour between the pristine laminate and the wrinkled one. The pristine laminate is characterized by a net load drop after failure, associated with the failure of the loaded side of the laminate which can be considered ripped off, while the wrinkled one is
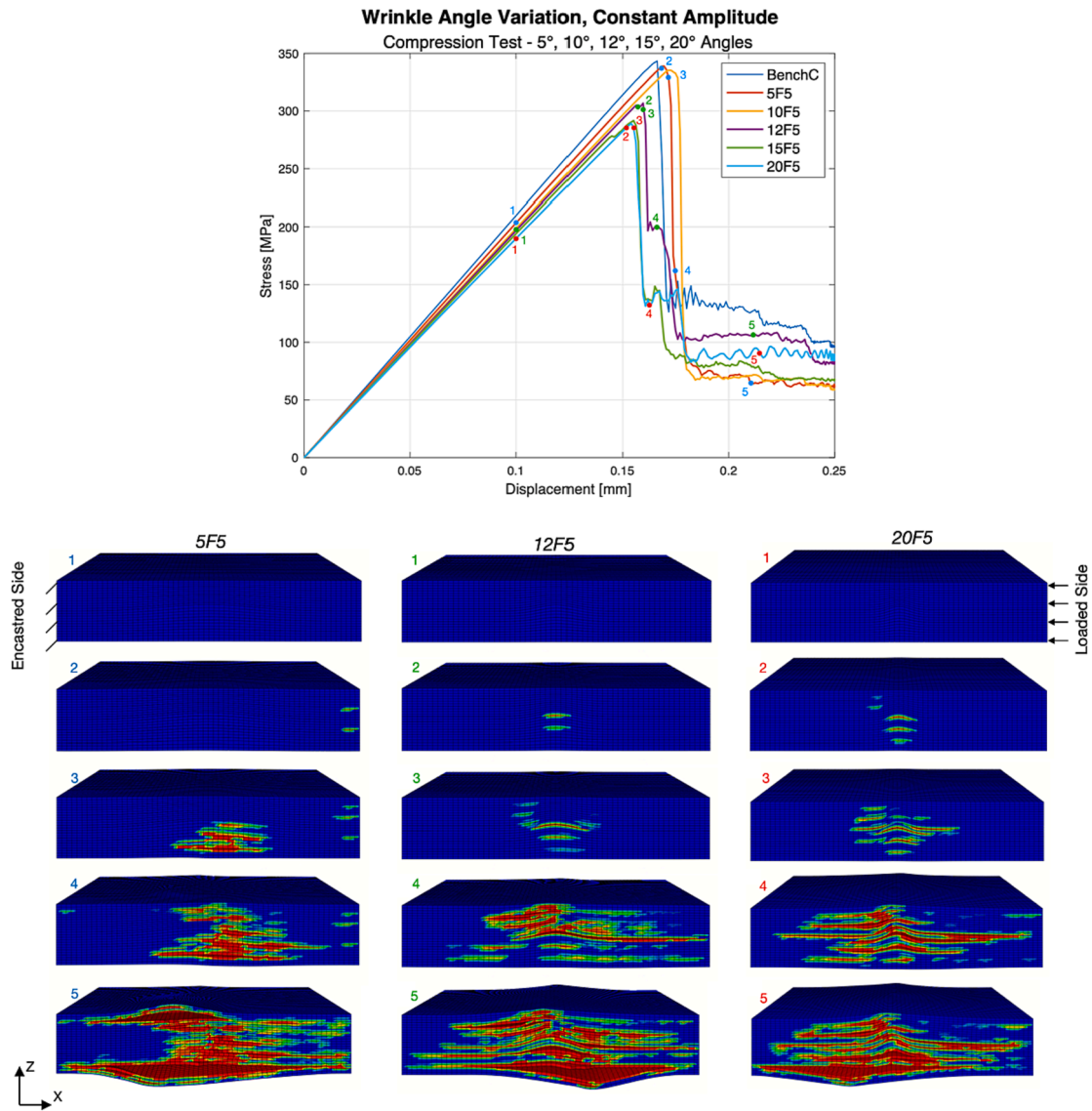
Fig. 10. Comparison of different wrinkle angles with 0.625 mm amplitude (compressive simulation).
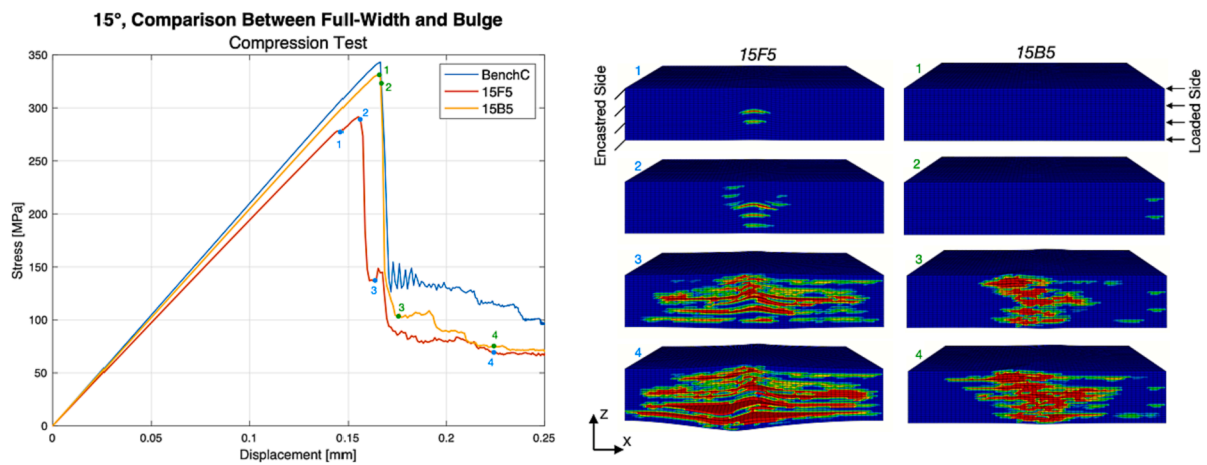

Fig. 11. Comparison between full-wave and bulge defects for the same wrinkle angle and amplitude (compressive simulation).
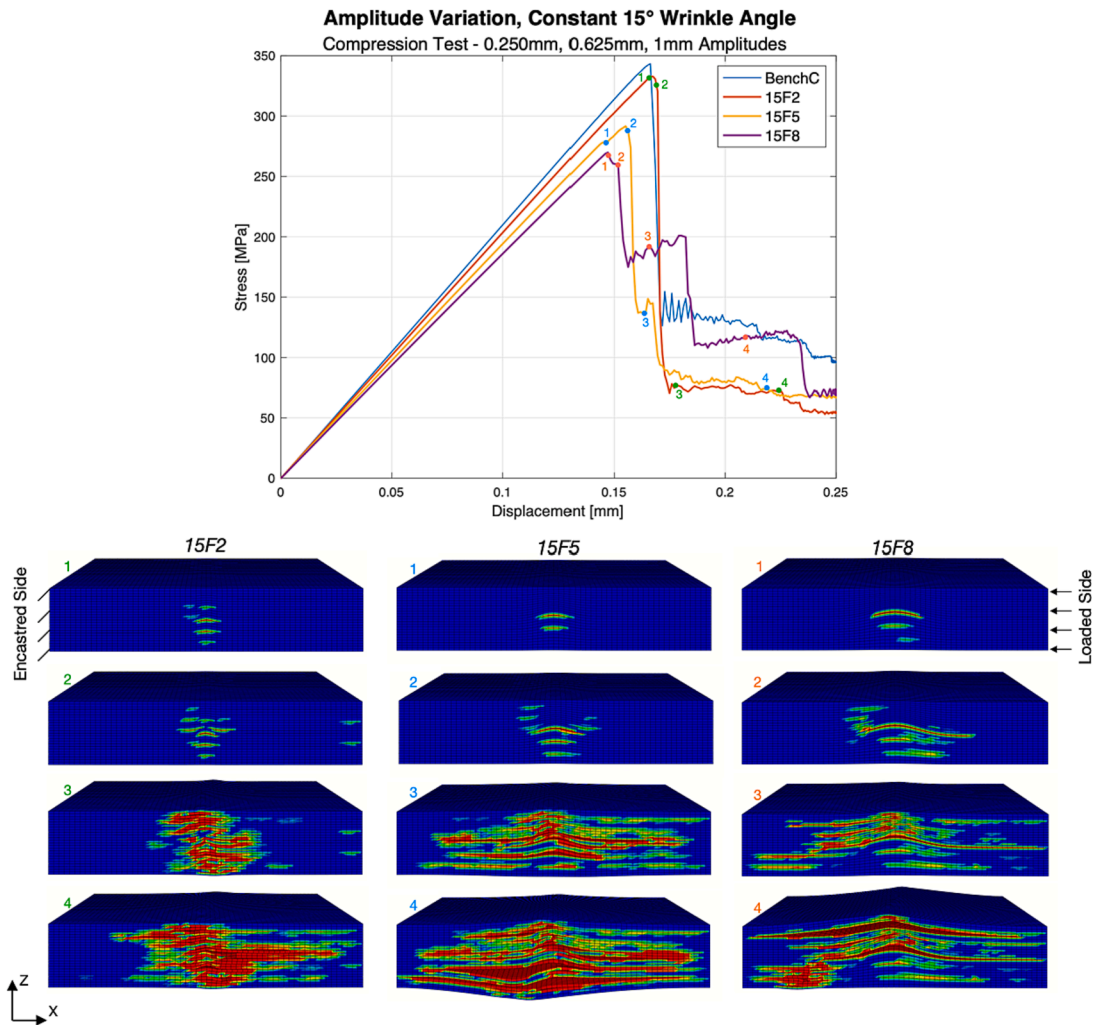
Fig. 12. Comparison of different amplitudes with the same 15° wrinkle angle (compressive simulation).
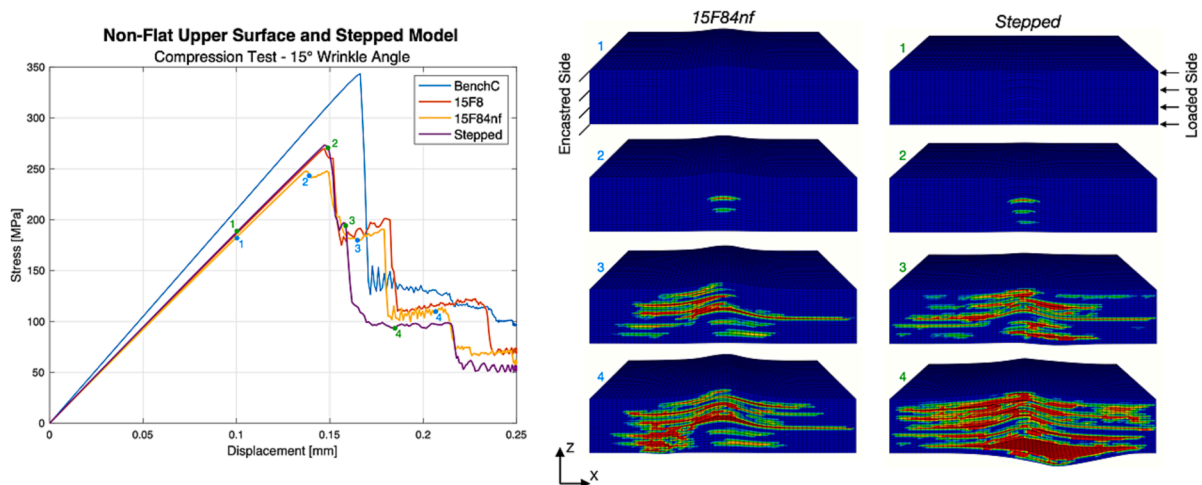

Fig. 13. Comparison between non-flat upper surface model and stepped model (compressive simulation).

characterized by successive small load drops each followed by a linear elastic region with diminished stiffness. The maximum compressive strength is diminished from the 469.3 MPa of the pristine laminate to the 379.4 MPa of the wrinkled one, showing therefore a 20.84% reduction in tensile strength for a 15° wrinkle with 0.625 mm wave amplitude.

Regarding the compressive tests of Fig. 9, the analysis of the stress-displacement plot shows a similar failure behaviour between both models. Both models achieve a clear load drop and show a slight constant decrease in load in the post-failure range, with small oscillations mainly due to vibrations in the material. The maximum compressive
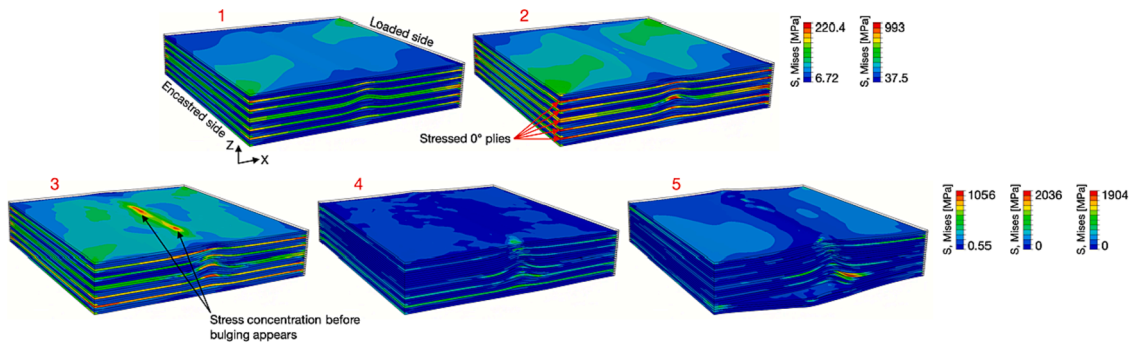
Fig. 14. Stress contour plot (S, Mises field variable) for 15° wrinkle angle with 0.625 mm maximum amplitude (15F5 model) at different simulation phases.
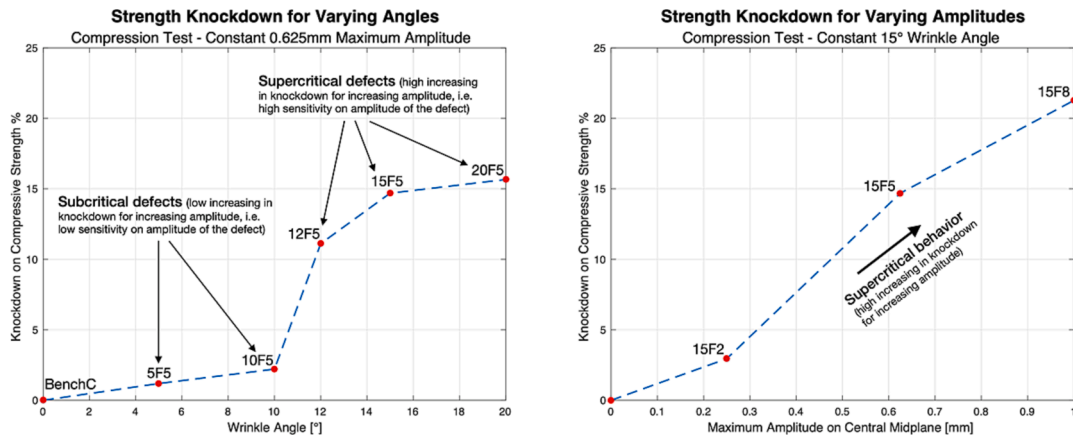

Fig. 15. (Left) knockdown on compressive strength for varying wrinkle angle and constant amplitude (second set); (right) knockdown on compressive strength for varying wave amplitude and constant angle (third set).

strength is diminished from 342.9 MPa of the pristine laminate to 291.6 MPa of the wrinkled one, showing therefore a 14.96% reduction in compressive strength for a 15° wrinkle with 0.625 mm wave amplitude. In both cases, lower stiffness is noticed for the wrinkled laminate in the elastic region compared to the benchmark model.

From the analysis of the compressive tests performed on the wrinkled laminate by modifying the wrinkle angle (Fig. 10 and Fig. 11) it is noticeable how the most consistent final delaminations happen on the external plies of the lower side, while the upper surface shows the inflexion correspondent to the wrinkle wave shape. The reason this failure mechanism happens is because the wave profile with linear amplitude variation shows thicker plies on the lower half of the laminate and thinner ones above. These upper plies are therefore subjected to stress concentrations which push the plies out-of-plane promoting a bulging and subsequently introducing localized delaminations below. This delamination then propagates through the interface as the applied displacement increases. For visualization purposes, stress contour plots for the 15° wrinkle angle at the phases selected and shown in Fig. 10 are displayed in Fig. 14. The initial stress affecting the 0° angle plies, and the successive concentrated stress strip visible on the upper bulging are noticeable from this image, the last one being a direct consequence of the upward push previously described.

It is concluded that the wrinkle shape has a clear effect on governing the damage onset and failure evolution scenarios. From the comparison of the various curves collected in Fig. 10, it is noticeable a general trend of diminishing compressive stiffness and strength for increasing angles, with failure strength values of 338.8 MPa for the 5° model, decreasing to 289.2 MPa for the 20° model.

As expected, a decrease in both the maximum compressive strength and stiffness with an increase in the angle is observed. However, the decrease of the compressive strength is not proportional to that of the

wave angle. In fact, for low angles (below 10°) a very low diminishing of failure strength is recorded, correspondent to 1.19% knockdown for 5° and 2.21% for 10°, while for higher angles the diminishing is more severe, with an 11.11% knockdown for 12°, 14.69% for 15° and 15.66% for 20°. Also, while for defects less than 10° the displacement at failure is slightly higher than that of the pristine laminate, for higher severity defects it is diminished. For visualization of these results, a plot of compressive strength knockdown versus wrinkle angle for constant maximum amplitude is shown on the left of Fig. 15.

It is hypothesized here that the nonlinear relationship between knockdown effect and angle is due to the dependence of compressive strength reduction for single-wave wrinkled laminates also on wave amplitude. Therefore other simulations belonging to the third set have been run, this time maintaining the same wrinkle angle of 15° but with three values of amplitude, i.e 0.250 mm, 0.625 mm and 1 mm, corresponding to 2, 5 and 8 times the original ply thickness values. As noticeable from the analysis of Fig. 12, for an increase in amplitude of the defect, which for fixed angle also corresponds to an increase of the defect wavelength, a clear decrease in compressive strength is recorded, with failure strength values of 332.8 MPa for the 0.250 mm amplitude defect, 291.6 MPa for the 0.625 mm amplitude one, and 270 MPa for the 1 mm one, correspondent to 2.95%, 14.69%, and 21.27% knockdowns, respectively, compared to the pristine laminate. The displacement at failure is also constantly diminished between the three simulations. As expected, initial failure mainly happens between the −45° and 0° plies, triggered by shear stresses. A plot of compressive strength knockdown versus maximum amplitude for constant wrinkle angle is shown on the right of Fig. 15.

An explanation of this nonlinear relationship between strength knockdown and wrinkle angle for a constant amplitude value, for a single full-wave type of defect, comes from the fact that the wrinkle
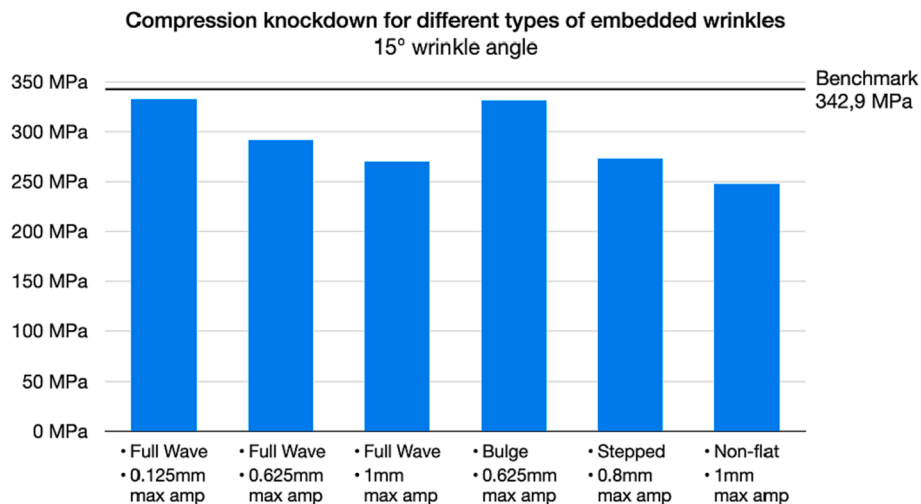
Fig. 16. Compressive strength values for different types of 15° wrinkle defects, compared to pristine laminate (benchmark model).

angle is not the only defining parameter as it is the combination of angle and amplitude that defines the severity of the knockdown effect. It is hypothesized that a critical aspect ratio exists between the defect's maximum amplitude value and wavelength in the load direction w_1, for which the sensitivity of the knockdown effect to the amplitude variation for a constant wrinkle angle is higher. Therefore, while for low angles (*subcritical defects* in Fig. 15) the increase of amplitude has a quasi-negligible effect on the knockdown in compressive strength, for higher angles (*supercritical defects* in Fig. 15, like the studied 15° one) small variations of amplitude produce tangible diminishing of the compressive strength. Caution should therefore be put when comparing the obtained results with those available in literature, since for the same angle different knockdown values can be found for different amplitudes. Similar results can be seen also in the work of Xie et al. [4], who found a sigmoidal relationship between knockdown and wrinkle angle. It is suggested here that this phenomenon requires a closer evaluation linking a number of real defects and confirming which parameter ranges produce realistic wrinkle defects before firm industrial guidance for NDT evaluations can be made.

Regarding the comparison between full-wave and bulge defects (Fig. 11), it is noticeable how for the same wrinkle angle and defect's amplitude, while a maximum compressive strength of 291.6 MPa is recorded for the full-wave defect, the bulge one show a higher value of 331.69 MPa. This represents a knockdown value of 3.27% for the bulge type defect compared with 14.69% for the full-wave one. It is believed that the reinforcing effect comes from the straight plies surrounding the defect which helps maintain a good effect on resisting compressive loads, while for the full-wave defect the entire cross-section is affected by the defect.

As for the comparison with experimental results found in the literature, the results of the simulations presented in Fig. 13 show that the non-flat upper surface model is affected by a clear knockdown in compressive strength due to the initial bulging, and reaches therefore a maximum stress of only 247.76 MPa corresponding to a knockdown of 27.74% compared to the pristine laminate. This is the highest knockdown that has been recorded in this study for a 15° wrinkle angle, and since it is due to the high amplitude in the central midplane, equal to 1 mm, and the initial bulge with the same fashion of the deformed shape, it represents an upper bound for the 15° wrinkle defect. The stepped model, on the other hand, shows a maximum compressive strength of 273.23 MPa, corresponding to a knockdown in compressive strength of 20.32% when compared to the pristine laminate. It should be noticed, however, that this model has been obtained by making the 90° plies as thin as possible (without reaching zero thickness values which are not physically possible, although 90° plies can be made thin in small regions

due to the disposition of fibres inside the resin matrix), and having groups of successive [-45°, 0°, 45°] plies ([-45°, 0°, 0°, 45°] in the central part of the laminate) with the same amplitude value. In this regard, by inputting a wrinkle angle of 15°, the maximum amplitude has been estimated to be 0.8 mm, which is slightly lower than 1 mm for the non-flat model (15F8 model used for comparison). It is noticeable that the stepped model with 0.8 mm amplitude behaves very similar to the linear model with 1 mm amplitude. It is therefore concluded that real defects in composite laminates, which are realistically more similar to the proposed stepped model than the idealized linear models studied, present slightly higher knockdown than those presented in this study, which are therefore underestimations. A comparison of the different strength values achieved for the 15° wrinkle defects is reported in Fig. 16 where it is noticeable the influence of defect type and amplitude for constant wrinkle angle.

4.1. Validation of the numerical models

The numerical results discussed in the previous section have been built following an approach of increased complexity: from basic defects belonging to the first three sets, realistic defects have been considered in Set 4 (*15F84nf* and *Stepped* models). As said, such last models mimic defects presents in manufactured specimens and are suitable for validating the proposed approach. For validating the proposed approach, experimental results have been found in the literature that are comparable to the square specimen and materials analyzed in this study. Mukhopadhyay et al. [14] manufactured rectangular composite specimens made of carbon-epoxy IM7/8552 material, with a quasi-isotropic $[45_2/90_2/-45_2/0_2]_{3S}$ stacking sequence and a nominal ply thickness of 0.125 mm, thus consistent with the models analyzed in this paper. Their specimen dimensions where 110 mm × 30 mm × 6 mm, with a gauge length of 30 mm. Wrinkling defects where induced during cure by inserting additional prepreg strips on 90° orientation on already existing 90° plies, effectively reproducing a quasi-stepped amplitude variation of the wrinkle defect. Their experimental results where then reproduced with a numerical model built in Abaqus/Explicit with an approach similar to the one presented in this paper. From experimental results, a knockdown of 30% has been obtained for a rectangular wrinkled specimen with a ∼ 12° wrinkle angle and a maximum amplitude estimated to be slightly above 1 mm. This result compares well with the proposed models, since the 12° angle is a supercritical one for such amplitude value and it can easily be estimated that for a maximum amplitude higher than 1 mm with a stepped variation the knockdown in compressive strength will be placed in the range between 20% and 30%, extrapolating the behaviours from preceding figures.

1) LAMINATE CONFIGURATION

2) WRINKLE GENERATION
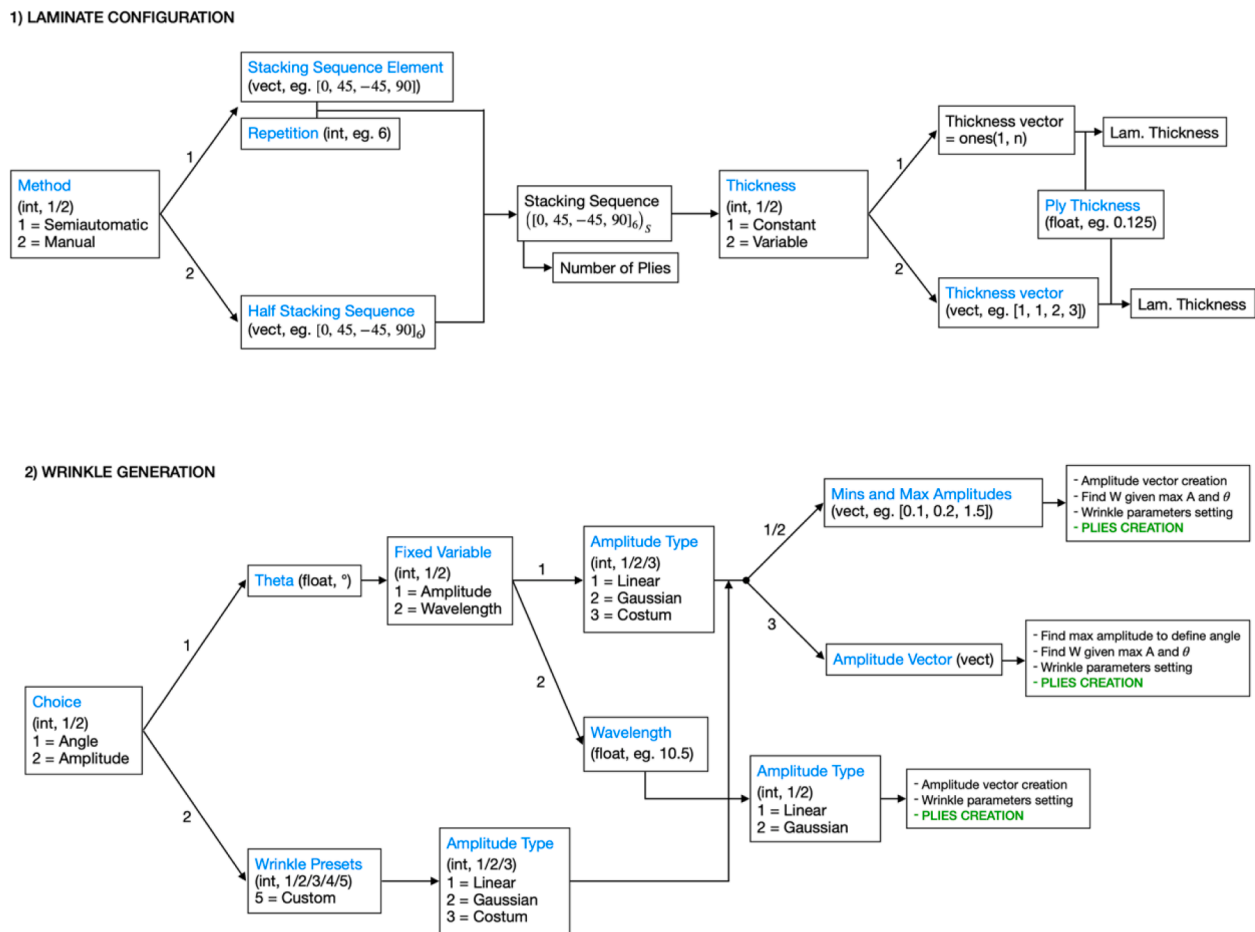
Fig. A1. Flowchart of the developed Matlab routine. 1) Laminate configuration process, 2) Wrinkle generation process. The two phases are intended to be completed in succession, by elaborating the inputs required to the user. The input file is then generated creating a numerical model based on the desired characteristics decided by the user.

Following such study, Xie et al. [4] proposed a numerical approach able to create FE models of wrinkle specimens starting from NDT data and a mathematical representation of the wrinkle defect's geometry. Their model implemented the same material properties, stacking sequence, ply thickness and side dimension of Mukhopadhyay et al. [14], thus being compatible with the models studied in the present paper. From numerical analyses, they found a 19% knockdown for 13° wrinkle angle and 33% knockdown for 18° wrinkle angle, both with stepped amplitude evolution. Additionally, as it has been highlighted before, they found a sigmoidal behaviour of knockdown increment for increasing angle and fixed amplitude, similar to the one presented in Fig. 15, again confirming the validity of the presented results.

From the good agreement with the aforementioned results, the results of the parametric study presented, the modelling procedure can be considered suitable giving confidence to the implemented Matlab routine as an effective tool in the study of wrinkled defects and their behaviours.

5. Conclusion

In this work, the effects of out-of-plane fibre waviness defects on the compressive behaviour of laminated composite specimens have been investigated from a numerical point of view. A mathematical formalization of the wave shape, which permits the definition of a wide variety of wrinkle defects through a small set of parameters, has been implemented in a Matlab-Abaqus FE routine, capable of generating several numerical models of wrinkled specimens. As composite laminates with embedded wrinkle defects subjected to compressive stress states show

complex failure mechanisms involving both intra-laminar and inter-laminar damages, intra-laminar damages have been considered by means of Hashin failure criteria, while for the onset of inter-laminar damages the Cohesive Zone Method (CZM) approach has been chosen, coupled with a quadratic damage initiation criterion, and a power-law criterion used to govern the mixed-mode behaviour damage evolution.

A range of parametric analyses has been conducted by selectively varying the wrinkle parameters to understand the relative influences of defect shapes and severities. In particular, variations of the wrinkle angle from 5° to 20° and of the wrinkle amplitude from 0.125 mm to 1 mm have been considered, as well as different types of wrinkles such as full-wave defects and bulge defects. Moreover, realistic defect characteristics have been addressed through the definition of stepped and non-flat models, which better represent manufacturing defects due to the autoclave process.

From the analysis of the obtained results, different conclusions can be drawn. It has been noticed how consistent delaminations happen on the external plies of the laminate, and a decrease of both the maximum compressive strength and stiffness with the increase of the angle has been observed. However, the relation has not been found to be proportional: it is in fact hypothesized that the nonlinear relationship between knockdown effect and angle is due to the dependence on wave amplitude of compressive strength reduction for single wave wrinkled laminates. As such, a critical aspect ratio exists between maximum amplitude value and wavelength in the load direction, for which the sensitivity of the knockdown effect to the amplitude variation for a constant wrinkle angle is higher. Moreover, it has been noticed that real defects in composite laminates, which are realistically more similar to
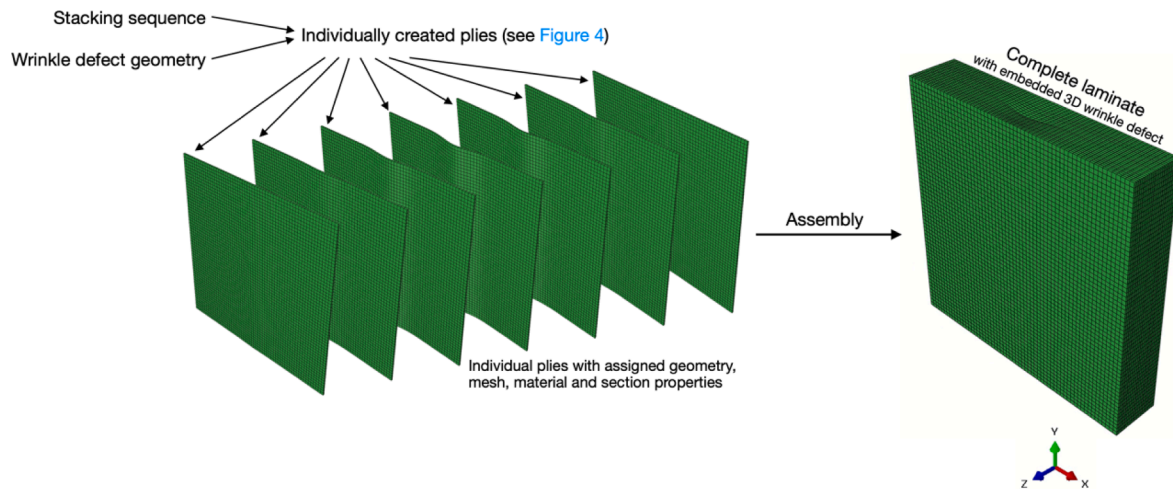
Fig. A2. Laminate creation based on assembly of individual plies. Plies are modelled as individual parts in Abaqus with assigned geometry, mesh, material and section properties and subsequently superimposed (stacked) on top of each other.

the proposed stepped model than the idealized linear models, present slightly higher knockdown than those presented in this study, which are therefore underestimations. Finally, a comparison with experimental validations found in the literature where similar models have been studied confirms that the implemented Matlab-Abaqus routine can be considered an effective tool in the study of wrinkled defects and their behaviours.

CRediT authorship contribution statement

Guglielmo Cimolai: Conceptualization, Methodology, Software, Investigation, Writing – original draft. **Mehdi Yasaee:** Methodology, Resources, Writing – review & editing, Supervision.

Declaration of Competing Interest

The authors declare that they have no known competing financial interests or personal relationships that could have appeared to influence the work reported in this paper.

Data availability

Data will be made available on request.

Appendix 1

Fig. A1

Appendix 2

Fig. A2

References

[1] Zhang J, Chevali VS, Wang H, Wang CH. Current status of carbon fiber and carbon fibre composites recycling. Comp B Eng 2020;193:108053.
[2] Hinton MJ, Kaddour AS, Soden PD. A comparison of the predictive capabilities of current failure theories for composite laminates, judged against experimental evidence. Compos Sci Technol 2002;62(12-13):1725–97.
[3] Soden PD, Hinton MJ, Kaddour AS. Biaxial test results for strength and deformation of a range of E-glass and carbon fibre reinforced composite laminates: failure exercise benchmark data. Compos Sci Technol 2002;62:1489–514.
[4] Xie N, Smith RA, Mukhopadhyay S, Hallett SR. A numerical study on the influence of composite wrinkle defect geometry on compressive strength. Mat Des 2018;140: 7–20.
[5] Potter KD. Understanding the origins of defects and variability in composites manufacture. In: 17th International conference on composite materials, Edinburgh International Convention Centre, Edinburgh, UK (2009) 27–31.

[6] Shi Y, Pinna C, Soutis C. Modelling impact damage in composite laminates: a simulation of intra- and inter-laminar cracking. Compos Struct 2014;114:10–9.
[7] Bloom LD, Wang J, Potter KD. Damage progression and defect sensitivity: an experimental study of representative wrinkles in tension. Compos B Eng 2013;45: 449–58.
[8] Potter K, Khan B, Wisnom M, Bell T, Stevens J. Variability, fibre waviness and misalignment in the determination of the properties of composite materials and structures. Compos A Appl Sci Manuf 2008;39(9):1343–54.
[9] Wang J, Potter KD, Hazra K, Wisnom MR. Experimental fabrication and characterization of out-of-plane fiber waviness in continuous fiber-reinforced composites. J Compos Mater 2012;46(17):2041–53.
[10] Adams DO, Hyer M. Effect of layer waviness on the compression strength of thermoplastic composite laminates. J Reinf Plast Compos 1993;12:414–29.
[11] Wisnom MR, Atkinson JW. Compressive failure due to shear instability: experimental investigation of waviness and correlation with analysis. J Reinf Plast Compos 1996;15(4):420–39.
[12] Bradley D, Adams D, Gascoigne H. Interlaminar strains and compressive strength reduction due to nested layer waviness in composite laminates. J Reinf Plast Compos 1998;17:989–1011.
[13] Lemanski SL, Wang J, Sutcliffe MPF, Potter KD, Wisnom MR. Modelling failure of composite specimens with defects under compression loading. Compos A Appl Sci Manuf 2013;48:26–36.
[14] Mukhopadhyay S, Jones MI, Hallett SR. Compressive failure of laminates containing an embedded wrinkle; experimental and numerical study. Compos A Appl Sci Manuf 2015;73:132–42.
[15] Ferreira LM, Graciani E, París F. Three dimensional finite element study of the behaviour and failure mechanism of non-crimp fabric composites under in-plane compression. Compos Struct 2016;149:106–13.
[16] Heuer H, Schulze M, Pooch M, Gäbler S, Nocke A, Bardl G, et al. Review on quality assurance along the CFRP value chain – non-destructive testing of fabrics, preforms and CFRP by HF radio wave techniques. Compos B Eng 2015;77:494–501.
[17] Sutcliffe MPF, Lemanski SL, Scott AE. Measurement of fibre waviness in industrial composite components. Compos Sci Technol 2012;72(16):2016–23.
[18] Smith RA, Mukhopadhyay S, Lawrie A, Hallett SR. Applications of ultrasonic NDT to aerospace composites. In: 5th Int. Symp. NDT Aerosp, Singapore; 2013. p. 1–12.
[19] Alghamdi AA, Mummery PM, Sheikh MA. Investigating the infuence of porosity on thermal and mechanical properties of a C/C composite using image based FE modelling. Int J Math Comput Phys Electr Comput Eng 2013;7:1–4.
[20] Makeev A, Nikishkov Y. *Material characterization and failure prediction for composites*, 37th Eur. Rotorcr. Forum: Milan, Italy; 2011. p. 1164–70.
[21] Freemantle R, Giannis S, Ják VMTÉ. Phased array data manipulation for damage tolerance assessment of composites using finite element analysis, 11th Eur. Conf. Non-Destructive Test 2014, 1–10.
[22] Sandhu A, Dodwell TJ, Butler R. An automated image processing algorithm to determine wrinkle characteristics from B-scans. In: 17th Eur. Conf. Compos. Mater., Munich, Germany; 2016. p. 1–8.
[23] Smith RA, Nelson LJ, Xie N, Fraij C, Hallett SR. Progressing 3D characterisation and modelling of monolithic carbon-fibre composites. Insight - Non-Destructive Test Cond Monit 2015;57:131–9.
[24] Hashin Z, Rotem A. A fatigue failure criterion for fiber reinforced materials. J Comp Mat 1973;7(4):448–64.
[25] Dugdale DS. Yielding of steel sheets containing slit. J Mech Phys Sol 1960;8(2): 100–4.
[26] Barenblatt GI. The mathematical theory of equilibrium cracks in brittle fracture. Adv App Mech 1962;7:55–129.
[27] Turon A, Camanho PP, Costa J, Dávila CG. A damage model for the simulation of delamination in advanced composites under variable-mode loading. Mech Mat 2006;38(11):1072–89.

[28] Camanho PP, Davila CG, De Moura Mf. Numerical simulation of mixed-mode progressive delamination in the composite materials. J Comp Mat 2003;37(16): 1415–38.

[29] Fedulov B, Antonov F, Safonov A, Ushakov A, Lomov S. Infuence of fibre misalignment and voids on composite laminate strength. J Compos Mater 2015;49: 2887–96.

[30] Hsiao HM, Daniel IM. Effect of fiber waviness on stiffness and strength reduction of unidirectional composites under compressive loading. Compos Sci Technol 1996; 56(5):581–93.

[31] Caiazzo A, Orlet M, McShane H, Strait L, Rachau C. The effects of marcel defects on composite structural properties. Compos Struct Theory Pract 2000;1383:158–87.

[32] El-Hajjar RF, Petersen DR. Gaussian function characterization of unnotched tension behavior in a carbon/epoxy composite containing localized fiber waviness. Compos Struct 2011;93(9):2400–8.

[33] Hexcel's HexPly® 8552 Product Data, available at: https://www.hexcel.com/user_area/content_media/raw/HexPly_8552_eu_DataSheet.pdf (accessed: 1 September 2022).

[34] Arhore EG, Yasaee M. Lay-up optimisation of fibre–metal laminates panels for maximum impact absorption. J Comp Mat 2020;54(29):4591–609.

[35] Zhang B, Kawashita LF, Jones MI, Lander JK, Hallett SR. An experimental and numerical investigation into damage mechanisms in tapered laminates under tensile loading. Comp A App Sci Manuf 2020;133:105862.

[36] Lapczyk I, Hurtado JA. Progressive damage modeling in fiber-reinforced materials. Compos A Appl Sci Manuf 2007;38(11):2333–41.

[37] Reinoso J, Blàzquez A, Estefani A, Parìs F, Canas J, Arèvalo E, et al. Experimental and three-dimensional global-local finite element analysis of a composite component including degradation process at the interface. Comp B Eng 2012;43: 1929–42.

[38] Koloor SSR, Tamin MN. Mode-II interlaminar fracture and crack-jump phenomenon in CFRP composite laminate materials. Compos Struct 2018;204: 594–606.

[39] Benzeggagh ML, Kenane M. Measurements of Mixed-Mode Delamination Fracture Toughness of Unidirectional Glass-Epoxy Composites with Mixed-Mode Bending Apparatus. Comp Sci Tech 1996;56:439–49.

[40] Weber TA, Englhard M, Arent J-C, Hausmann J. An experimental characterization of wrinkling generated during prepreg autoclave manufacturing using caul plates. J Comp Mat 2019;53(26-27):3757–73.